AGU PUBLICATIONS

JGR

Journal of Geophysical Research: Solid Earth

RESEARCH ARTICLE

10.1002/2015JB012447

Key Points:
- The smallest repeating earthquakes ever identified as such on geological faults
- They are likely repeat ruptures of asperities induced by creep of the surrounding fault
- They repeated much more frequently than those at plate boundaries for a given amount of creep

Supporting Information:
- Captions of Figures S1–S5
- Figure S1
- Figure S2
- Figure S3
- Figure S4
- Figure S5

Correspondence to:
M. Naoi,
naoi.makoto.4z@kyoto-u.ac.jp

Citation:
Naoi, M., et al. (2015), Unexpectedly frequent occurrence of very small repeating earthquakes ($-5.1 \le M_w \le -3.6$) in a South African gold mine: Implications for monitoring intraplate faults, *J. Geophys. Res. Solid Earth*, *120*, doi:10.1002/2015JB012447.

Received 13 AUG 2015
Accepted 16 NOV 2015
Accepted article online 18 NOV 2015

Unexpectedly frequent occurrence of very small repeating earthquakes ($-5.1 \le M_w \le -3.6$) in a South African gold mine: Implications for monitoring intraplate faults

Makoto Naoi[1], Masao Nakatani[2], Toshihiro Igarashi[2], Kenshiro Otsuki[3], Yasuo Yabe[4], Thabang Kgarume[5], Osamu Murakami[6], Thabang Masakale[7], Luiz Ribeiro[8], Anthony Ward[8], Hirokazu Moriya[9], Hironori Kawakata[10], Shigeru Nakao[11], Raymond Durrheim[5,12], and Hiroshi Ogasawara[10]

[1]Department of Civil and Earth Resources Engineering, Graduate School of Engineering, Kyoto University, Kyoto, Japan, [2]Earthquake Research Institute, Tokyo University, Tokyo, Japan, [3]Department of Earth Science, Graduate School of Science, Tohoku University, Sendai, Japan, [4]Research Center for Prediction of Earthquakes and Volcanic Eruptions, Graduate School of Science, Tohoku University, Sendai, Japan, [5]Council for Scientific and Industrial Research, Pretoria, South Africa, [6]Research Organization of Science and Engineering, Ritsumeikan University, Kyoto, Japan, [7]Open House Management Solutions, Potchefstroom, South Africa, [8]SeismoGen Cc, Carletonville, South Africa, [9]Graduate School of Engineering, Tohoku University, Sendai, Japan, [10]College of Science and Engineering, Ritsumeikan University, Kyoto, Japan, [11]Department of Earth and Environmental Science, Kagoshima University, Kagoshima, Japan, [12]School of Geosciences, University of the Witwatersrand, Johannesburg, South Africa

Abstract We observed very small repeating earthquakes with $-5.1 \le M_w \le -3.6$ on a geological fault at 1 km depth in a gold mine in South Africa. Of the 851 acoustic emissions that occurred on the fault during the 2 month analysis period, 45% were identified as repeaters on the basis of waveform similarity and relative locations. They occurred steadily at the same location with similar magnitudes, analogous to repeaters at plate boundaries, suggesting that they are repeat ruptures of the same asperity loaded by the surrounding aseismic slip (background creep). Application of the Nadeau and Johnson (1998) empirical formula (NJ formula), which relates the amount of background creep and repeater activity and is well established for plate boundary faults, to the present case yielded an impossibly large estimate of the background creep. This means that the presently studied repeaters were produced more efficiently, for a given amount of background creep, than expected from the NJ formula. When combined with an independently estimated average stress drop of 16 MPa, which is not particularly high, it suggests that the small asperities of the presently studied repeaters had a high seismic coupling (almost unity), in contrast to one physical interpretation of the plate boundary repeaters. The productivity of such repeaters, per unit background creep, is expected to increase strongly as smaller repeaters are considered ($\propto M_o^{-1/3}$ as opposed to $M_o^{-1/6}$ of the NJ formula), which may be usable to estimate very slow creep that may occur on intraplate faults.

1. Introduction

Microearthquakes that repeatedly occur at the same location with similar waveforms are observed at many plate boundaries [e.g., *Nadeau and Johnson*, 1998; *Matsuzawa et al.,* 2002]. They are called "repeating earthquakes" and thought to represent the repeat ruptures of the same asperity loaded by the surrounding aseismic slip (hereinafter referred to as "background creep"). The slip amount at the asperity, or the "repeater patch", must be the same as that of the background creep if a long period is considered, so the occurrence rate of such repeaters should be proportional to the background creep rate. Conversely, repeaters can be used to estimate the amount of background aseismic slip [e.g., *Igarashi et al.,* 2003; *Igarashi*, 2010; *Uchida et al.,* 2003, 2004, 2009; *Uchida and Matsuzawa*, 2011].

It may, therefore, be natural to expect that the background slip amount can be estimated by summing up coseismic slips at each repeater patch. This idea corresponds to the assumption that repeater patches slip only seismically. Under this assumption, if repeaters have coseismic stress drops in the range of 0.1–100 MPa (hereinafter referred to as the "normal stress drop range") independent of their magnitude, as normal (i.e., nonrepeater) earthquakes do [hereinafter referred to as "Constant Stress Drop (CSD) scaling"; e.g., *Aki*, 1972; *McGarr*, 1999;

Ide and Beroza, 2001; *Ide et al.,* 2003; *Yamada et al.,* 2005, 2007; *Allmann and Shearer*, 2007; *Kwiatek et al.,* 2011; *Yoshimitsu et al.,* 2014], the amount of the background creep (= cumulative amount of coseismic slips) allocated for each repeater recurrence should be proportional to the cube root of the seismic moment M_o of the repeater.

Nadeau and Johnson [1998], however, derived an empirical relationship inconsistent with the above idea. They have shown

$$\log d_b = -2.36 + 0.17 \ \log M_o, \tag{1}$$

where M_o is the seismic moment (dyne·cm) of the considered repeater, d_b is the amount of the background creep (cm) during one cycle of the repeater. Equation (1) (hereinafter referred to as the NJ formula) implies that d_b is proportional to $M_o^{1/6}$ ($\sim M_o^{0.17}$), not $M_o^{1/3}$. Equation (1) was obtained from a direct comparison between the background creep amount evaluated from geodetic observations and the occurrence rate of the repeaters in individual groups in the Parkfield region, California. It has been repeatedly demonstrated that the NJ formula is applicable to the repeaters at different plate boundaries, not only the Parkfield region [*Igarashi et al.,* 2003; *Chen et al.,* 2007, 2008; *Yu*, 2013].

To explain the NJ formula, an additional or different assumption is required. For example, if we keep the assumption that the repeater patches slip only seismically, the coseismic stress drop (and, therefore, the coseismic slip amount) expected from the NJ formula is much larger than that expected from the CSD scaling for small repeaters (hereinafter referred to as "tight-patch NJ model"). Some previous studies suggested that small repeaters do have very high stress drops [*Nadeau and Johnson*, 1998; *Johnson and Nadeau*, 2002; *Dreger et al.,* 2007]. In contrast, other researchers have suggested that the discrepancy from the CSD scaling is only apparent, resulting from significant aseismic slip at the repeater patch; seismic coupling of the repeater patches χ_{patch} is low, especially for small repeaters [*Beeler et al.,* 2001; *Chen and Lapusta*, 2009]. In this model (hereinafter referred to as "loose-patch NJ model"), the CSD scaling and the NJ formula hold at the same time.

Actually, repeaters not following the NJ formula have been reported, though cases are few. *Hiramatsu et al.* [2011] and *Hayashi and Hiramatsu* [2013] found repeaters among aftershocks of large intraplate earthquakes that were likely induced by afterslip. They suggested that the amount of the background creep estimated from the simple sum of coseismic slips, which was much less than calculated from the NJ formula, was likely more appropriate. It is important to know what type of repeaters follows the NJ formula partly because this likely reflects the physics and/or the environment of the source of repeating earthquakes and partly because this affects the validity of the estimation of the background aseismic slip. Such verification is easier for smaller repeaters because the discrepancy between the NJ formula and the CSD scaling becomes larger due to the different scaling exponents of M_o.

In the present study, we analyze very small repeating earthquakes ($-5.1 \le M_w \le -3.6$) found on a geological fault that was monitored by an AE (acoustic emission) network at 1 km depth in the Cooke 4 mine, South Africa [*Naoi et al.,* 2014]. Although *Naoi et al.* [2015a] have already shown some examples of larger repeating AEs ($-2.5 \le M_w \le -2.1$) in another planar cluster detected by the same network, the present study focuses on AEs that occurred on another fault closer to the AE network. Because of the higher network sensitivity and location accuracy, we were able to identify a large number of smaller repeaters, which have a higher occurrence rate than the larger ones. We confirmed that they were definitely repeaters through observations of more than 10 cycles, in the best cases. We were also able to estimate the corner frequency and stress drop of the repeaters, which allowed us to estimate the coseismic slip amount of the repeaters and thereby evaluate the relation between the repeater activity and the background creep. Although direct geodetic measurements of the background creep are lacking, we have some qualitative constraints.

2. Observation of Acoustic Emissions at 1 km Depth in the Cooke 4 Mine

Figure 1 shows our observation network in the Cooke 4 mine. We installed 24 highly sensitive AE sensors (red and green circles in Figure 1), 6 triaxial accelerometers (not shown), and two 3-component Ishii strainmeters (cyan squares in Figure 1) [*Ishii et al.,* 1997] in boreholes drilled from the tunnels at 1 km depth [*Naoi et al.,* 2014; *Ogasawara*, 2013]. These sensors surrounded a part of a geological fault called the "Zebra fault," whose position and attitude were precisely evaluated by borehole logging, core observation, and observation of exposures in mining tunnels (see *Naoi et al.* [2015b] for details). A subhorizontal planar mining area advancing northward

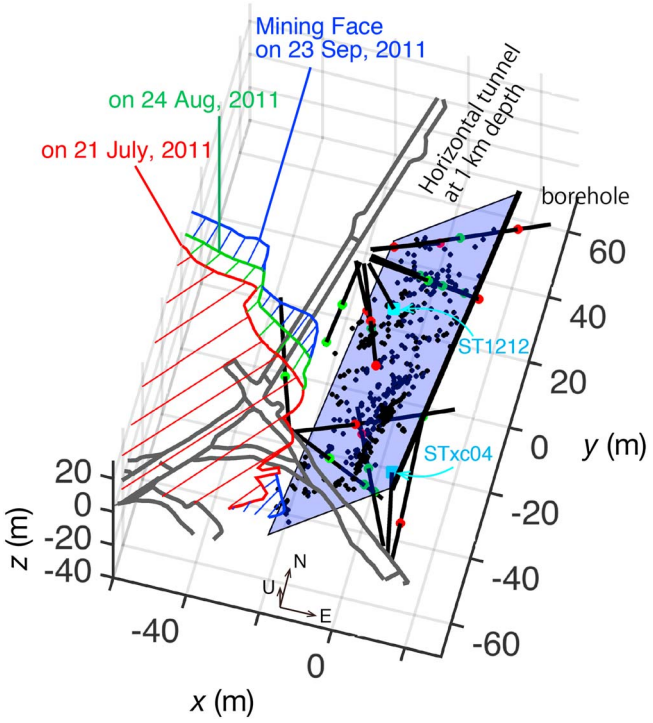

Figure 1. Observation network deployed at 1 km beneath the ground in the Cooke 4 mine, South Africa. The origin of *x* and *y* coordinates coincides with the geometrical center of gravity of the AE network. The origin of the *z* coordinate is taken at the depth of the tunnel (gray line) from which the network was deployed. Blue plane: the approximation plane of the planar AE alignment (black circles) along the Zebra fault determined by *Naoi et al.* [2015b] (See *Naoi et al.* [2014, 2015b] for details of the overall AE distribution around the site). Red circles denote the AE sensors that were used to calculate cross-correlation coefficients in identification of repeaters (section 3), while green circles denote the remaining AE sensors. Cyan squares denote 3-component strainmeters. Red, green, and blue contours and hatches indicate the mining faces and the mined-out cavities, as of 21 July, 24 August, and 23 September, 2011, respectively.

lay about 20 m above the horizontal tunnels (~30 m or more away from the Zebra fault), building up the stress around the site.

The AE sensors record seismic signals with workable signal-to-noise (S/N) ratios up to ~50 kHz, although that varies with the signal intensity. When a predetermined trigger condition is met at any one channel, waveform data of 65.5 ms duration are recorded for all the AE sensors and the accelerometers at a rate of 500 kHz. The waveforms are analog high pass filtered at 1 kHz for the AE sensors and at 50 Hz for the accelerometers before analog to digital conversion. See *Naoi et al.* [2014, 2015a, 2015b] for details of the AE observations. The strainmeters measure strain changes in three directions separated by 120°, all perpendicular to the borehole axis, recorded continuously at 40 Hz.

Naoi et al. [2014] applied the automatic traveltime detection software of *Horiuchi et al.* [2011] to waveform records produced by 150 million triggers obtained by the AE network during a period of 2 months from 6:32:22 on 8 August 2011 to 9:54:58 on 10 October 2011 and determined their hypocenters from *P* and *S* arrival time readings assuming a homogeneous medium with $V_P = 5700$ m/s and $V_S = 3600$ m/s. We choose 365,237 well-located events that have at least 10 *P* wave arrival time readings and root-mean-square traveltime residuals of 0.2 ms or less. We next estimated the seismic moment M_o and the moment magnitude M_w for the events by fitting the theoretical spectra of the ω^2 model to the spectra of AE records and accelerograms, after correcting for the frequency characteristics of the AE sensors calibrated in situ against neighboring accelerometers. The M_o and M_w were determined for ~98% events, and the minimum M_w was -5.3. See *Naoi et al.* [2014] for details of the catalog development procedure, including M_o and M_w estimation.

The AEs cataloged by *Naoi et al.* [2014] can be classified into two populations: the "stope cluster", which occurred just ahead (within ~20 m) of the advancing mining faces and comprises 90% of all AEs and the "planar clusters", which exhibited two-dimensional distributions and are situated at greater distances (up to ~100 m) from the mining face. *Naoi et al.* [2015b] relocated the planar-cluster AEs by using the double difference method [*Waldhauser and Ellsworth*, 2000] with the cross-correlation traveltime reading technique and reported several sharp, planar aggregations within a thickness of several decimeters, likely delineating fracture interfaces with macroscopic displacement discontinuities. Some of the clusters were consistent with mapped faults, including the Zebra fault [*Naoi et al.,* 2015b]. Figure 1 shows 851 AEs that were allocated to the Zebra fault (AEs located within 4 m of the approximate plane are shown in Figure 1. See *Naoi et al.* [2015b] for details of the cluster identification). The composite focal mechanism evaluated from *P* wave first motions of the AEs was consistent with a normal slip on the Zebra fault, implying that most of them occurred on the fault [*Naoi et al.,* 2015b].

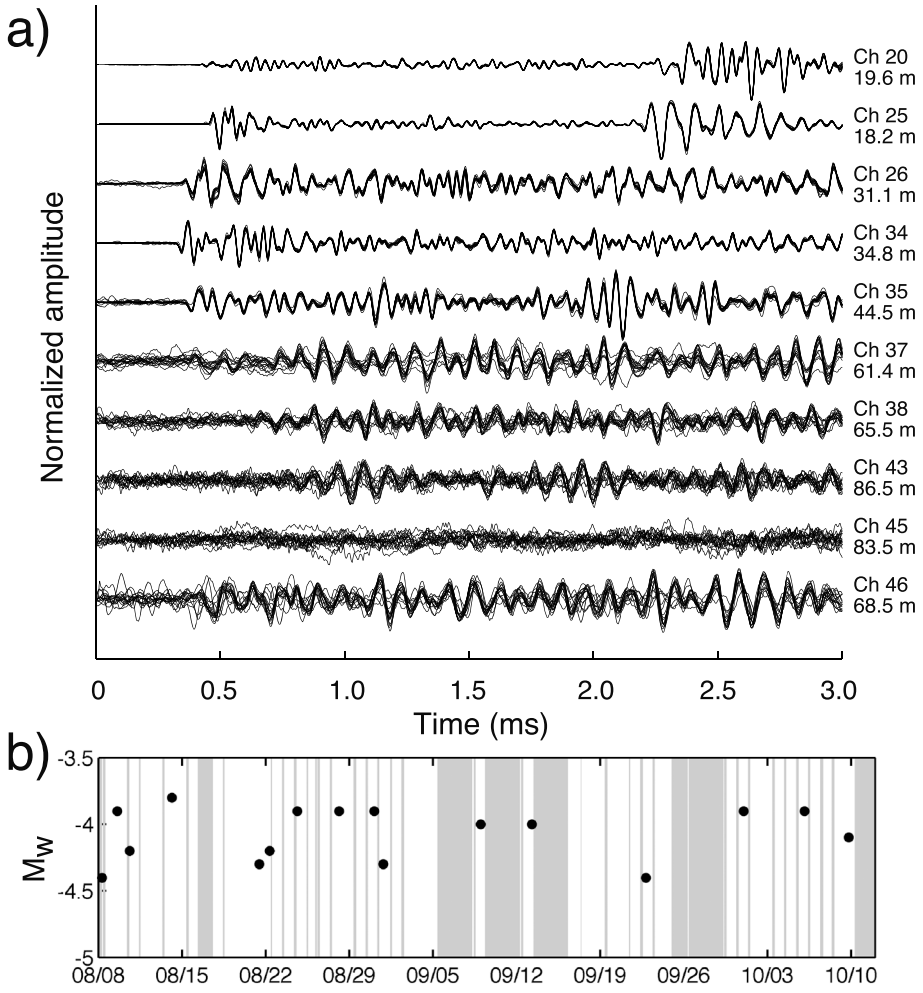

Figure 2. (a) Waveforms of AEs belonging to the largest repeater group identified in section 3. Normalized waveforms of the 16 repeater events recorded at the 10 AE sensors used for repeater identification (red circles in Figure 1) are plotted. Waveforms recorded at each station are overlaid. The distance between the sensor and the repeater patch is shown to the right of the waveforms from each sensor. (b) Magnitude-time diagrams for the group. Gray shades indicate missing data periods. Examples of some other groups are shown in Figures S1–S5.

3. Identification of Repeater Groups

We searched for repeating earthquakes among the 851 AEs on the Zebra fault, which occurred steadily during the analysis period [*Naoi et al.,* 2015b]. This activity consisted of only very small AEs, with a maximum M_w of −3.1.

Repeater groups were identified by the following procedures. We cross-correlated waveforms of all event pairs whose interevent distances D were less than 2 m on the basis of the relocated hypocenters in *Naoi et al.* [2015b]. We used band-pass-filtered (0.1–100 kHz) waveforms of 10 AE sensors (red circles in Figure 1) from 0.4 ms before the P wave onset to 1.5 times the S-P time after the onset. We did not calculate the cross-correlation coefficient C_c for stations when the S/N ratios for both events were smaller than 3 so as to avoid spuriously large C_c that may be produced by local noise sources recorded by nearby stations.

We then chose event pairs whose C_c was greater than 0.90 at two or more stations and event-separation distance D was less than $0.5r_{lg}$, where r_{lg} is the rupture radius evaluated from the M_o of the larger of the pair, assuming a stress drop of 16 MPa. The assumed value of 16 MPa is the logarithmic average of stress drops for repeaters in the study described here (section 4). The latter criterion allowed us to select event

Table 1. Dependency of Repeater Grouping on the Criteria for Identification[a]

	Criteria				Results					
Line	Cc Threshold	Minimum Number of High C_C Stations	Maximum Event Separation to Calculate C_C	Assumed Stress Drop (MPa)	Number of Repeater Group	Number of Events in the Largest Group	Number of Repeaters	Percentage of Repeaters	Background Creep (CSD) (mm)	Background Creep (NJ) (mm)
1	0.9	**1**	$0.5r_{ig}$	16	111	16	386	45.4	0.0090–0.19	2.7–35
2	0.9	**2**	$0.5r_{ig}$	16	111	16	386	45.4	0.0090–0.19	2.7–35
3	0.9	**3**	$0.5r_{ig}$	16	111	16	386	45.4	0.0090–0.19	2.7–35
4	0.9	**4**	$0.5r_{ig}$	16	109	16	376	44.2	0.0090–0.19	2.7–35
5	0.9	**5**	$0.5r_{ig}$	16	85	15	299	35.1	0.0095–0.18	2.8–33
6	**0.85**	2	$0.5r_{ig}$	16	111	16	386	45.4	0.0090–0.19	2.7–35
7	**0.9**	2	$0.5r_{ig}$	16	111	16	386	45.4	0.0090–0.19	2.7–35
8	**0.95**	2	$0.5r_{ig}$	16	110	16	380	44.7	0.0090–0.19	2.7–35
9	0.9	2	$0.5r_{ig}$	**0.1**	127	22	459	53.9	0.00031–0.0093	2.7–49
10	0.9	2	$0.5r_{ig}$	**1**	117	22	427	50.2	0.0014–0.043	2.7–49
11	0.9	2	$0.5r_{ig}$	**16**	111	16	386	45.4	0.0090–0.19	2.7–35
12	0.9	2	$0.5r_{ig}$	**100**	92	16	297	34.9	0.026–0.65	2.5–35
13	0.85	1	∞	0.1	137	22	506	59.5	0.00029–0.0093	2.6–49
14	0.95	5	$0.5r_{ig}$	100	54	12	168	19.7	0.041–0.47	3.1–24

[a]The studied parameters are shown in bold in each line.

pairs whose rupture areas overlapped significantly. In the estimation of fault radius r, we used the equation

$$r^3 = \frac{7}{16}\frac{M_o}{\Delta\tau}, \quad (2)$$

where $\Delta\tau$ is the stress drop [*Eshelby*, 1957; *Keilis-Borok*, 1959; *Kanamori and Anderson*, 1975]. The selected pairs were then assembled into "repeater groups" when they shared one event or more. We identified a total of 111 repeater groups consisting of 2–16 AEs. Of the 851 events, 386 events (45%) belonged to one of the groups. If the analysis period is extended, some of the remaining 55% AEs may be judged to be repeaters. The magnitude of the repeaters was in the range $-5.1 \leq M_w \leq -3.6$. To date, they are the smallest repeating earthquakes identified as such on a geological fault, including repeaters found in mines [*Yamamoto*, 2008; *Yoshimitsu et al.*, 2012; *Naoi et al.*, 2015a]. Figure 2a shows waveforms of the 10 AE sensors that were used in the repeater identification for all the 16 events belonging to the largest repeater group, showing the very high similarity of waveforms among events belonging to the same group, though the similarity become lower for more distant stations owing to low S/N ratios. Examples of some other groups are shown in Figures S1–S5 in the supporting information.

Different criteria for repeater identification yield different grouping results, of course. Table 1 shows the dependency of the grouping results on the minimum number of stations with high C_c (Lines 1–5), the threshold of C_c (Lines 6 and 7), and the assumed stress drop used to calculate rupture radius (Lines 9–12). The number of repeater groups meeting the criteria decreases when the minimum number of stations is greater than 3 or minimum C_c increased to 0.95. A 1000-fold increase in the assumed stress drop (which affects the rupture radius and hence the event separation criterion) decreases the number of repeater groups from 127 to 92. Line 13 shows a case with very slack criteria, while Line 14 shows a case with stringent criteria. Even in these extreme cases, the number of repeaters only differs from the base case (Line 2) by a factor of about 2, which does not affect the arguments of the present paper.

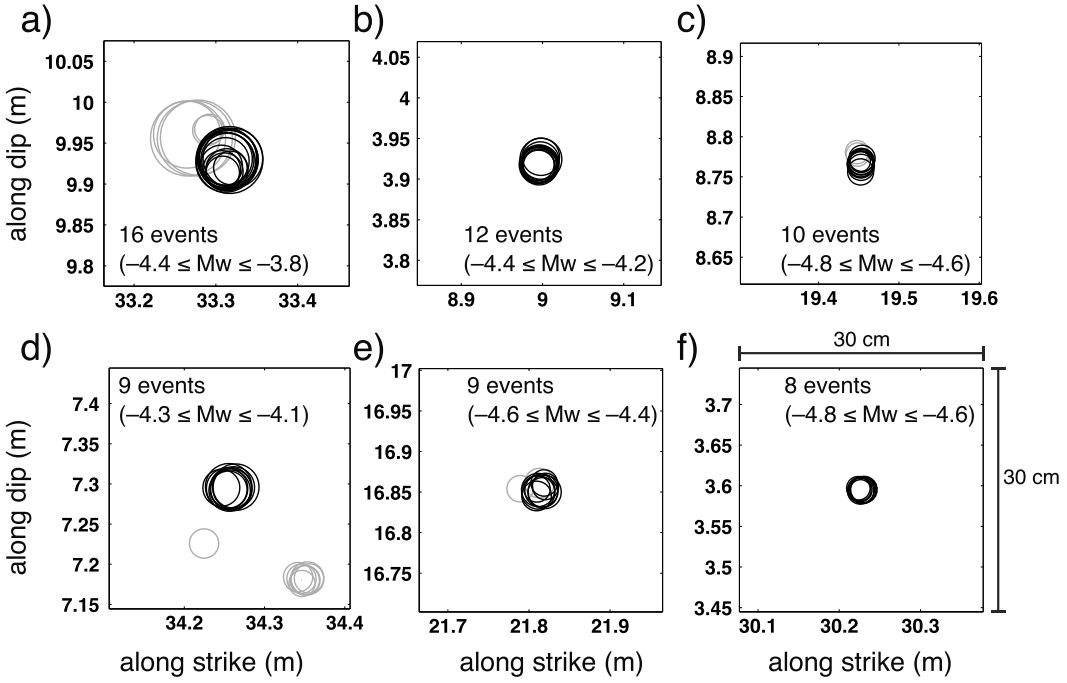

Figure 3. Estimated rupture areas of the repeating AEs that belong to the six largest groups. The rupture areas are projected onto the blue plane shown in Figure 1 by using the same coordinate system as that of Figure 4. Black circles indicate AEs belonging to the repeater group that is focused on in each panel, while gray circles indicate others including AEs belonging to other repeater groups. (a–f) The centers of the plot area correspond to the center of gravity of the event locations shown by black circles. Rupture areas were calculated from equation (2) with an assumed stress drop of 16 MPa.

Figures 2b and S1b–S5b show magnitude-time diagrams for the six largest groups. The AEs in each repeater group tend to occur steadily with similar magnitudes, although some long intervals, probably due to missing data periods, are recognized. These features are in common with the repeating earthquakes at plate boundaries, suggesting the same basic mechanism for repeating ruptures. That is, the repeating earthquakes found in the present study are likely to be the ruptures of asperities on the fault repeatedly loaded by the surrounding long-term background creep. In support of this interpretation, *Naoi et al.* [2015b] provided evidence that they were on-fault events with slip direction favored by the vertical-compression stress state on the Zebra fault as suggested by in situ absolute stress measurements near the site by an overcoring technique [*Ogasawara et al.,* 2014].

Figure 3 shows the rupture areas of the AEs belonging to the six groups. The rupture areas were evaluated from equation (2) with a stress drop of 16 MPa. The AEs that ruptured almost the same area were well grouped. Especially, the group shown in the center of Figure 3a was clearly distinguished from the close neighboring group.

Scatterings among the hypocenters of almost colocated events suggest that typical relative location error ranges from a few millimeters to 1.5 cm. For example, all AEs in the $30 \times 30\,\mathrm{cm}^2$ area shown in Figures 3b and 3f are co located within only 9 mm. The location of all AEs shown in Figures 3c and 3e were also very close to each other, but in each figure, two were classified to another group or labeled as isolated (gray circles) due to their slightly different positions that did not satisfy the $D < 0.5r_{\mathrm{lg}}$ condition. Actually, these gray-colored events have large C_c (>0.9) with respect to the black-colored events at several stations, so they may well be repeat ruptures of the same patch as that of the black-colored events; their slightly different positions may simply result from location errors that were slightly larger than typical values. The criterion of $D < 0.5r_{\mathrm{lg}}$ might be too strict in this sense, but we use this criterion so as to register only the events that definitely represent repeat ruptures of the same patch.

Figure 4a shows the hypocenter distribution of the repeaters and isolated AEs (i.e., AEs not belonging to any repeater groups), while Figure 4b shows their space-time diagram. Both types of AEs occurred steadily during

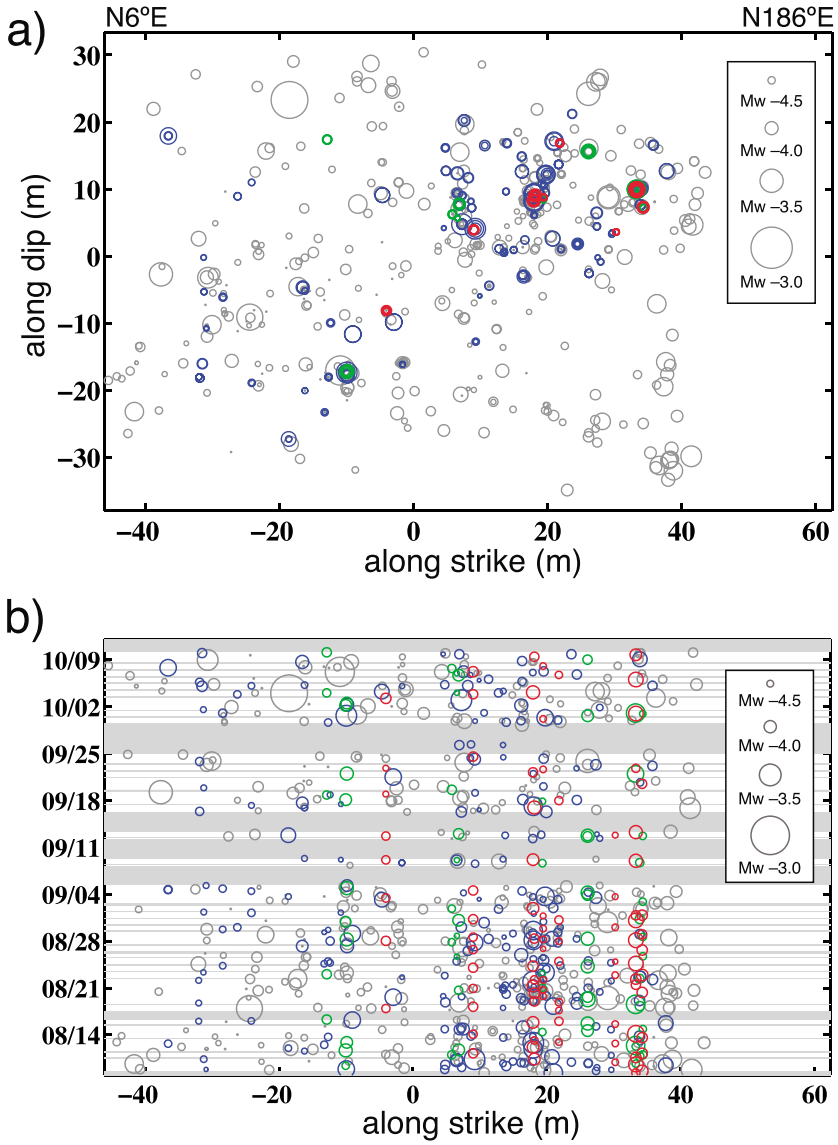

Figure 4. (a) Hypocenter distribution of the repeating AEs on the Zebra fault. The diameter of each circle is 30 times the source diameter estimated from equation (2) assuming a stress drop of 16 MPa. Red circles: AEs belonging to repeater groups having eight or more members (9 groups). Green circles: AEs belonging to the groups having 5–7 members (12 groups). Blue circles: AEs belonging to the groups having 2–4 members (90 groups). Gray circles: AEs not belonging to any repeater groups. Dots indicate events whose M_W could not be determined. (b) Space-time diagram of the repeating AEs. The same coloring and sizing rules were used as Figures 4a for circles and dots representing AEs.

the analysis period over the cluster extent (~$100 \times 70\ m^2$), implying that the background creep over the broad region lasted for more than 2 months, though the activity rate of the AEs in the cluster seems somewhat higher in August than in the later period (Figure 4b).

4. Coseismic Stress Drops of the Repeating Earthquakes

We estimated the corner frequency f_c and the stress drop $\Delta\tau$ of the repeaters identified in section 3 by using the multiple empirical Green's function (MEGF) method of *Ide et al.* [2003], which is a slight modification of the *Hough* [1997] method. In this approach, f_c and their relative seismic moments for multiple events are simultaneously estimated by fitting the theoretical ratio of Fourier amplitude spectra to the observed ones.

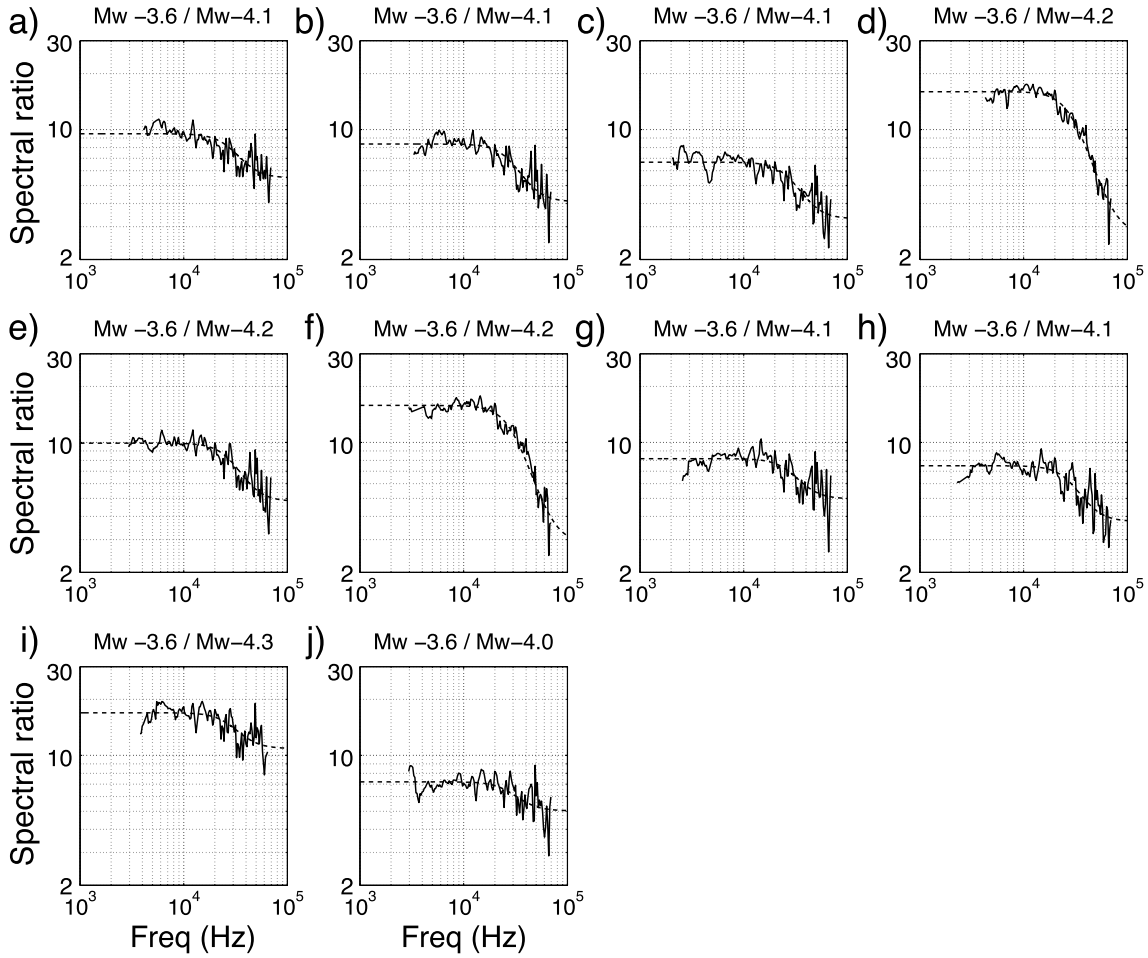

Figure 5. Spectral ratios of event 13 (Table 2; M_w −3.6) with respect to 10 nearby smaller events ($-4.3 \le M_w \le -4.0$). Results shown are after averaging over many stations and time windows (solid line). Dashed lines are the theoretical spectra calculated with the inverted corner frequency and relative seismic moment.

The spectral ratio for each event pair was calculated by an approach similar to *Uchida et al.* [2012]. First, for all the 24 AE sensors, we calculated amplitude spectra for the *P* wave train of each event, using five tapered windows of 1.3 ms in length, each overlapping the next one by 20% of its duration (0.26 ms). Later windows were discarded if they included the *S* wave. We then resampled the spectra at equal log-frequency intervals in a range of 1–70 kHz and removed the frequency components that had an insufficient S/N ratio (<10).

After excluding the spectra from stations whose event-station distance was less than 30 times the inter event distances (so as to exclude event pairs that have different paths), we took spectral ratios for individual stations and windows. We obtained up to 120 spectral ratios (24 stations × 5 windows) for each event pair. They were stacked at each frequency bin to compose a ratio spectrum that will be fitted to invert f_c of the event pair by the MEGF method. In the inversion of f_c, we did not use the spectral ratio of frequency bins built from the stack of fewer than 10 spectral ratios (as opposed to the ideal case of 120 ratios).

The f_c analysis by the MEGF method was conducted for 35 events selected by the following procedure. First, we grouped event pairs whose cross-correlation coefficient C_c calculated in section 3 was greater than 0.70 at two or more stations. We call these "spectral ratio groups" to distinguish them from the repeater groups. We adopted a smaller threshold for C_c than in section 3 and did not apply a restriction in interevent distance. This is to allow each group to have events with significantly different f_c, which is prerequisite for the MEGF method. We next selected 35 events with $M_w \ge 4.0$ that were accompanied by mates smaller by 0.3 or more in M_w. These 35 events belonged to 16 spectral ratio groups.

Table 2. Source Parameters of Repeating AEs

No	Repeater Group ID[a]	Trigger Time	M_w	f_c (kHz)	r (cm)	Stress Drop (MPa)	x (m)[b]	y (m)[b]
1	1	2011 Aug 09 13:47:29.343	−3.9	37.3	3.7	15.1	33.32	9.93
2	1	2011 Aug 14 03:33:33.390	−3.8	37.5	3.7	21.7	33.32	9.93
3	1	2011 Aug 24 15:30:35.796	−3.9	39.6	3.5	18.1	33.31	9.93
4	1	2011 Aug 28 03:05:56.156	−3.9	40.0	3.5	18.7	33.32	9.93
5	1	2011 Aug 31 02:07:56.140	−3.9	36.2	3.8	13.8	33.31	9.93
6	1	2011 Sep 30 23:54:05.031	−3.9	39.5	3.5	17.9	33.32	9.93
7	1	2011 Oct 06 01:59:05.640	−3.9	48.9	2.8	34.0	33.31	9.93
8	10	2011 Aug 19 07:07:54.906	−3.9	25.4	5.5	4.8	26.11	15.62
9	12	2011 Aug 12 09:13:47.640	−3.7	21.2	6.5	5.6	33.28	9.96
10	12	2011 Aug 18 13:17:04.656	−3.7	27.8	5.0	12.4	33.27	9.96
11	12	2011 Sep 21 23:36:13.984	−3.8	49.6	2.8	50.0	33.26	9.96
12	12	2011 Oct 01 01:46:48.343	−3.7	48.5	2.9	66.1	33.27	9.96
13	22	2011 Oct 02 23:55:10.296	−3.6	26.1	5.3	14.6	7.24	4.76
14	30	2011 Oct 07 20:21:26.203	−3.8	31.8	4.4	13.3	−36.58	17.94
15	31	2011 Aug 08 07:26:56.734	−3.7	32.8	4.2	20.4	20.97	17.14
16	31	2011 Aug 18 06:39:40.031	−3.8	36.0	3.9	19.2	20.98	17.14
17	37	2011 Aug 10 07:54:56.703	−3.6	27.4	5.1	16.9	9.21	4.08
18	39	2011 Aug 11 21:01:00.421	−3.7	18.1	7.7	3.5	17.97	8.20
19	39	2011 Aug 21 22:06:52.093	−3.6	29.4	4.7	20.8	17.97	8.20
20	39	2011 Aug 29 13:48:21.234	−3.7	27.3	5.1	11.8	17.97	8.20
21	41	2011 Oct 09 02:31:39.328	−3.9	30.2	4.6	8.0	33.91	10.07
22	41	2011 Aug 23 07:07:51.921	−3.7	30.4	4.6	16.3	19.75	12.17
23	41	2011 Sep 03 16:17:52.843	−3.7	30.3	4.6	16.1	19.75	12.16
24	52	2011 Sep 30 08:58:44.953	−3.8	34.4	4.0	16.8	19.75	12.16
25	53	2011 Aug 12 19:27:26.984	−3.6	30.3	4.6	22.9	17.99	9.30
26	53	2011 Aug 28 02:25:44.468	−3.7	27.7	5.0	12.3	17.98	9.31
27	53	2011 Sep 17 03:27:28.109	−3.7	33.1	4.2	21.1	17.99	9.30
28	–	2011 Oct 08 23:56:52.906	−3.6	30.7	4.5	23.7	−30.67	−3.22

[a]Numbers 1–27 are identified as repeating earthquakes in section 3.
[b]x is hypocenter position along strike in the coordinate system used in Figure 4a, and y is along dip.

We then estimated the f_c of the 35 events by using those mates in each group as empirical Green's functions. In the f_c estimation, the f_c was obtained for the smaller mates as well. They were, however, unlikely to be reliable as their estimated f_c tended to be near the upper limit of the used frequency range (70 kHz), so we did not use them in the subsequent analyses. In addition, we labeled the estimation unsuccessful if $\log_{10}(dR)$ was smaller than 0.3 for all event pairs used in the estimation, where dR is the ratio of amplitudes at the high- and low-frequency limits of the inverted spectral ratio (i.e., nearly flat spectral ratios were obtained for all event pairs) and also labeled unsuccessful if $\log_{10}(df)$ is smaller than 0.5, where df is the ratio between the estimated f_c, and the lower limit of the frequency band used for the spectrum fitting (small df corresponds to the lack of flat part lower than f_c). After the screening, we obtained f_c for 28 events ($-3.9 \le M_w \le -3.6$), which included 27 of the repeaters (from 11 repeater groups) defined in section 3.

Figure 5 shows examples of spectral ratios between an M_w −3.6 AE occurring on 2 October 2011 and neighboring events ($-4.3 \le M_w \le -4.0$) that were used as empirical Green's functions. The observed spectra ratios are well fitted by the theoretical curves.

We then evaluated the fault radius r by using the circular crack model of *Sato and Hirasawa* [1973] assuming a rupture velocity of 90% of the S wave velocity and evaluated stress drops $\Delta\tau$ by using equation (2). In the calculation, we used the estimates of M_o in the catalog (section 2; also see Appendix A about the reliability of our M_o estimation). The resultant f_c, r, and $\Delta\tau$ for the 28 events are listed in Table 2. The range of $\Delta\tau$ was 3.5–66 MPa, with a logarithmic average of 16 MPa. This comfortably falls within the normal stress drop range of earthquakes (0.1–100 MPa; see section 1).

5. Creep on the Zebra Fault

We now examine the applicability of equation (1), the NJ formula, to the Zebra-fault repeaters. Figure 6a shows the amount of creep during the 2 month analysis period estimated by equation (1) for the 111 repeater

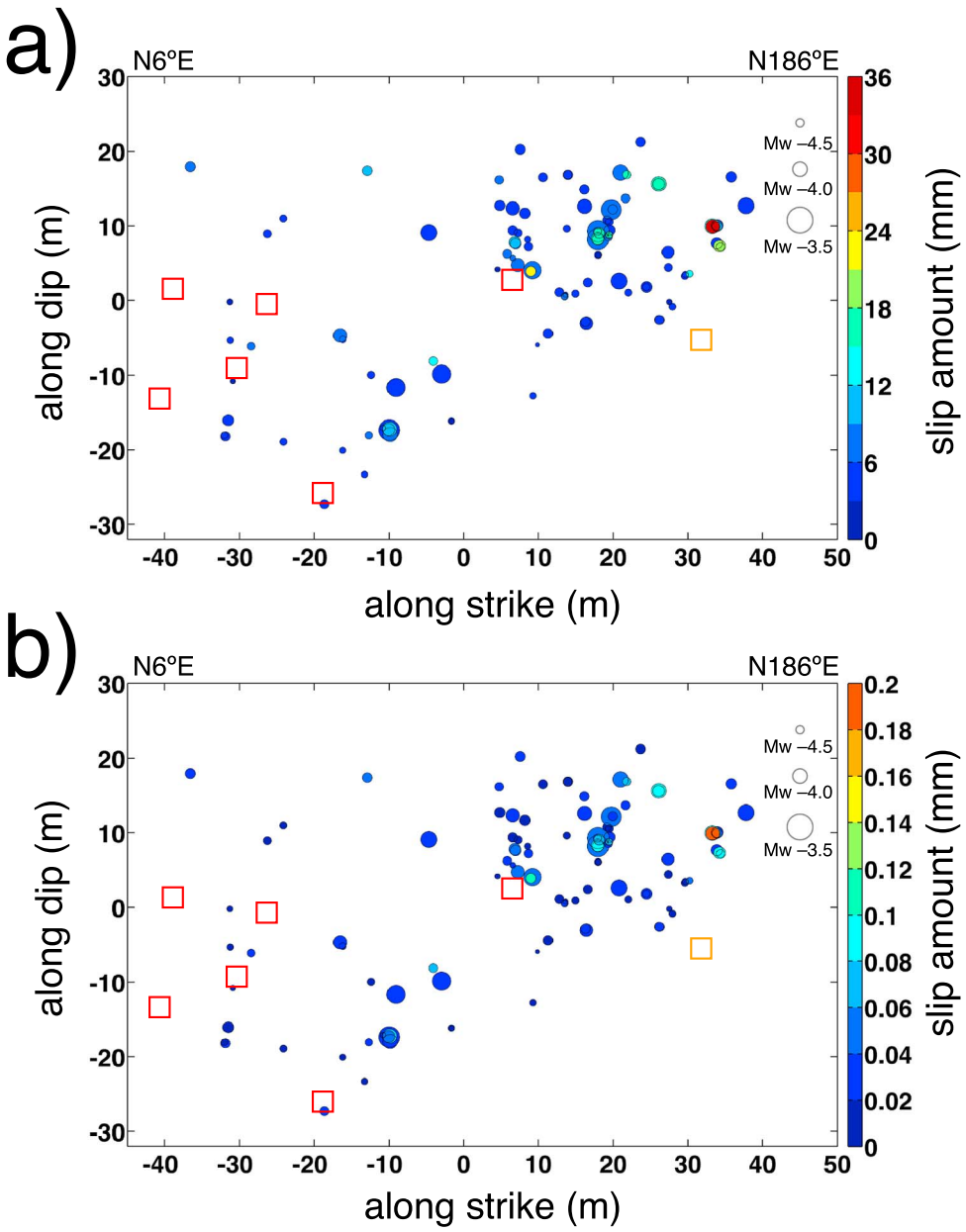

Figure 6. Cumulative slip amount during the 2 months, estimated for each repeater patch. Each circle represents a repeater group. The diameter of the circles is drawn 30 times greater than the source diameter estimated from equation (2) with a 16 MPa stress drop and the average seismic moment of the events in each group. Squares indicate the position of the intersection between the Zebra fault and the boreholes in which sensors are installed. Red: boreholes in which the cables remained sound as of the end of August 2013. Orange: signals through the cable in the borehole were lost in June 2012. Postmortem analyses suggest that the loss of signals in the case was caused by the deterioration of the electronics due to water leaking into the sensor package cemented in the borehole (mild shorting, which indicates cable is intact). (a) Results based on the NJ formula (equation (1)). The obtained cumulative slip amount is 2.7–35 mm. (b) Cumulative sum of coseismic slips estimated from the constant stress drop scaling (16 MPa assumed). The obtained cumulative slip amount is 0.009–0.19 mm.

groups. We obtained 2.7–35 mm of creep amount, depending on the repeater group, during the 2 months. This is the minimum estimation from the NJ formula, partly because of the strict criterion to select repeaters (section 3) and partly because of missed repeaters that fell in the missing data periods (gray hatches in Figures 2b and 4b). The large variation of the estimated slip amount (about 1 order of magnitude) among groups is likely attributable to missed repeaters.

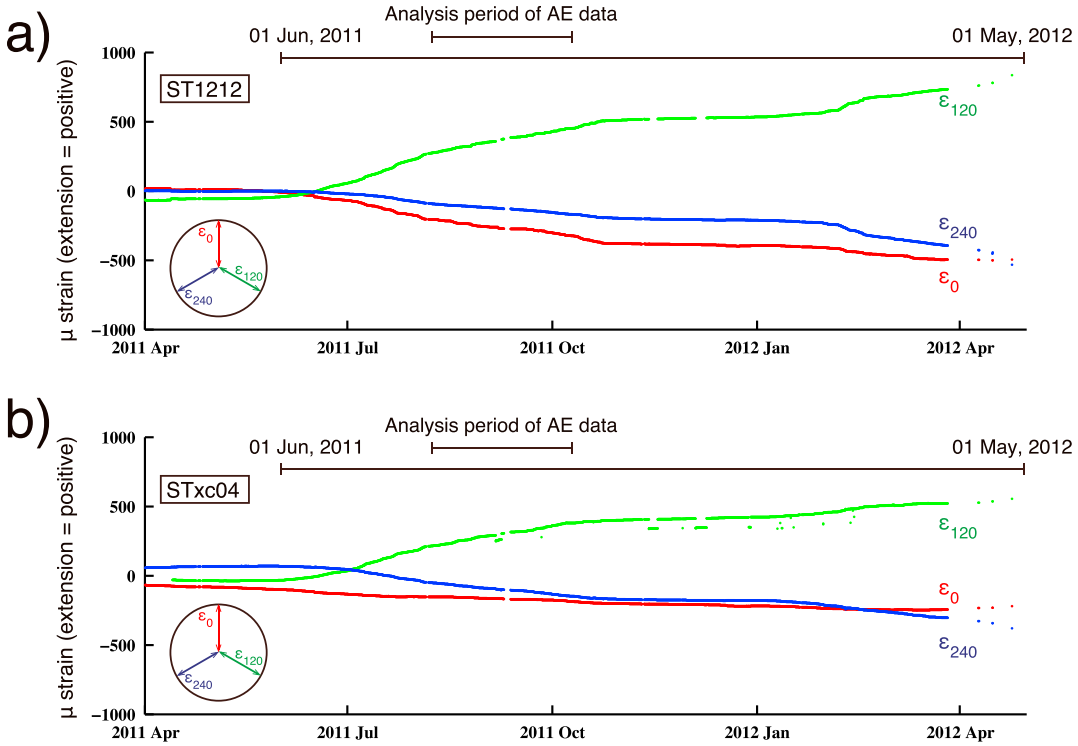

Figure 7. Records of two 3-component strainmeters installed near the Zebra fault. The positions of the instruments are shown in Figure 1. (a) Results for ST1212, installed in the hangingwall side of the Zebra fault. (b) Results for STxc04, installed in the footwall side. These strainmeters record the strain components of ε_0, ε_{120}, and ε_{240} in the plane normal to the borehole axis (inset; orientation of the strain components viewed from the South).

Despite being the minimum estimation, these are deemed far too large for the creep amount during the 2 months. Sensor cables were cemented in the 60 mm diameter boreholes, and some of them go through the fault (squares in Figure 6), so that a creep of more than ~10 mm would have damaged the cables. However, such damage by borehole dislocation did not happen. For example, a cable in a borehole intersecting the fault at a point near (~3 m) the repeater patch at (along dip, along strike) = (8.996 m, 3.919 m), where a background creep of 22.6 mm was estimated for the 2 months (shown by a yellow circle), was still functional, transmitting good AE signals as of August 2013 (2 years after the start of the analysis period). In addition, two strainmeters installed near the fault (Figure 1) indicated that the rock mass strain, and hence, the stress accumulation around the fault lasted for 11 month period from June 2011 to May 2012 (Figure 7), which includes the 2 month period of our repeater analysis. Hence, the creep of the Zebra fault probably continued for a period much longer than the 2 months, and many more repeaters must have occurred during the long period in which the cables going through the fault survived. We therefore conclude that the background creep rate of the Zebra fault was much less than expected from the NJ formula.

On the other hand, we obtain a cumulative slip of 0.009–0.19 mm by summing up coseismic slips estimated from the CSD scaling with an assumed stress drop of 16 MPa, approximately the logarithmic average of the stress drops estimated in section 4 (Figure 6b). Here the fault radius r was calculated from equation (2), and the coseismic slip d_s was calculated from the equation

$$M_o = \mu d_s S = \pi \mu r^2 d_s, \tag{3}$$

where, μ is the rigidity (assuming 30 GPa), and S is the area of the rupture ($S = \pi r^2$). This estimate gives a lower bound of the background creep, which corresponds to a case where the repeaters occur at fully coupled ($\chi_{\text{patch}} = 1$) patches. The estimated order of creep rate is small enough to be consistent with the observed survival of our cables. The actual amount of the background creep is probably closer to Figure 6b than Figure 6a. In the following discussions, we therefore assume that the seismic coupling at the repeater patches on the Zebra fault is high, probably almost unity.

6. Discussion

6.1. Comparison With the Models for the NJ Formula

As reviewed in section 1, it has been suggested that the NJ formula results from the tendency that smaller repeaters have either larger coseismic stress drop (tight-patch NJ model) or smaller seismic coupling χ_{patch} (loose-patch NJ model). These tendencies should become extreme for very small repeaters. Although the repeaters on the Zebra fault did not obey the NJ formula (section 5), we check quantitatively how these parameters differ between the Zebra repeaters and those obeying the NJ formula.

First, we try calculating $\Delta\tau$ expected of the tight-patch NJ model, where a repeater patch slips only seismically. Under this assumption, *Nadeau and Johnson* [1998] proposed the relation between seismic moment M_o [dyne · cm] and coseismic stress drop $\Delta\tau$ [bar]:

$$\log \Delta\tau = 8.19–0.25 \log M_o. \tag{4}$$

For M_w −4 repeaters, as small as the ones on the Zebra fault, we get an extremely high stress drop of ~50 GPa, 3 orders of magnitude greater than the range estimated in section 4.

Second, we try calculating χ_{patch} assuming the loose-patch NJ model, where significant amount of aseismic slip occurs at the patch. This can be calculated from the ratio between the coseismic slip amount estimated from the CSD scaling ($\Delta\tau = 16$ MPa assumed) and the background creep amount estimated from the NJ formula. For M_w −4 repeaters, very low coupling of $\chi_{\text{patch}} \sim 0.006$ is implied. This is much smaller than the χ_{patch} on the Zebra fault, as discussed in section 5. These big differences suggest vastly different physical conditions at the repeater patches on the Zebra fault and the cases that follow the NJ formula, typically seen at plate boundaries.

6.2. Implications for Detection of Very Slow Background Creep

In the following discussion, we use the term "mine-type repeater" to denote repeaters that have stress drop in the normal stress drop range and occur at patches of χ_{patch} ~1. Background creep associated with mine-type repeaters can be estimated from the sum of coseismic slip of the repeaters estimated from the CSD scaling. As discussed earlier, the present case of the Zebra repeaters provides a suitable example.

The high stress drop in the tight-patch NJ model and the small χ_{patch} in the loose-patch NJ model were introduced to compensate for the deficiency of the cumulative coseismic-slip amount estimated from the CSD scaling compared with the background creep amount evaluated from geodetic observation. In other words, in the NJ formula, the background creep amount allocated to one repeater cycle is greater than mine-type repeaters; conversely, a given amount of background creep generates more mine-type repeaters than the ones following the NJ formula.

Mine-type repeaters thus give us an opportunity to detect very slow fault creep in a short observation period. Figure 8a shows the relation between the rate of background creep and the recurrence interval T_R of mine-type repeaters. We may evaluate T_R by the equation:

$$T_R = \frac{d(M_o)}{V_c}, \tag{5}$$

where V_c is the background creep rate and d is the background creep amount allocated for one repeater cycle. For mine-type repeaters, $d(M_o)$ is given by the following equation, which is derived from equations (2) and (3):

$$d(M_o) = \frac{Mo}{\pi\mu}\left(\frac{16}{7}\frac{\Delta\tau}{M_o}\right)^{\frac{2}{3}}. \tag{6}$$

Figure 8a is drawn assuming a stress drop of 16 MPa. We also show the same diagram for repeaters obeying the NJ formula in Figure 8b, where $d(M_o)$ is given by d_b in equation (1). From these diagrams, we can find how long an observation period is needed to detect the fault creep of a given rate by waiting for the recurrence of a repeater with a given M_w. For example, in the case of Figure 8a, by looking at M_w −4 repeaters, one can detect a fault creep of 0.03 mm/year (corresponding to seismic coupling of 97–99.7% for a Class-A fault, whose geological slip rate is 1–10 mm/year, under the assumption of a constant creeping rate over the entire

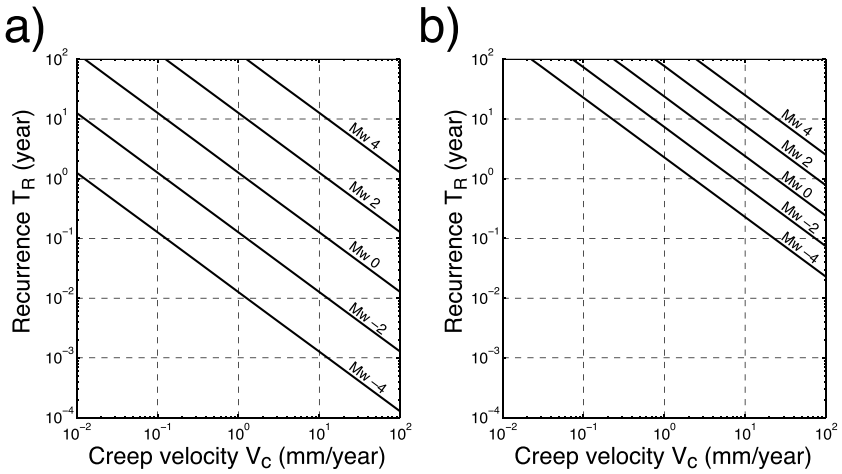

Figure 8. Relation between the recurrence interval of repeating earthquakes and the background creep velocity. (a) For mine-type repeaters (section 6.2) with a stress drop of 16 MPa. (b) For repeaters following the NJ formula (equation (1)).

interval between major earthquakes) by ~0.4 year of observation, whereas it takes ~76 years for a repeater of the same magnitude to repeat once according to the NJ formula (Figure 8b).

For tectonic earthquakes, *Hiramatsu et al.* [2011] and *Hayashi and Hiramatsu* [2013] reported repeating earthquakes for which the NJ formula overestimates the background creep, similarly to the present case of Zebra repeaters. Those repeaters occurred in the aftershock sequences of two intraplate earthquakes, the 2007 Noto Hanto earthquake and the 2000 Western Tottori earthquake. They interpreted that these repeaters were induced by afterslip of their respective main shocks. In contrast, the NJ formula has been validated well for repeaters at plate boundaries as reviewed in section 1. Although we cannot obtain firm conclusions due to an insufficient number of cases, it appears that repeaters at plate boundaries follow the NJ formula, while those on intraplate faults do not, in the sense that repeaters occur more often for a given amount of background creep. This difference might be somehow related to the physical states of faults that are differently conditioned according to, for example, the overall coupling and/or the geologic slip rate of the fault.

If creep on intraplate faults generates mine-type repeaters, very slow creep, which cannot be detected by today's geodetic observation, can be measured in a relativity short period by observation of very small repeaters. Then intraplate faults may become amenable to repeater-based analyses currently limited to plate boundaries, for example, estimation of the spatial distribution of fault coupling [e.g., *Igarashi et al.,* 2003; *Igarashi*, 2010; *Uchida et al.,* 2003, 2004, 2009; *Uchida and Matsuzawa*, 2011] and monitoring of transient aseismic slip [e.g., *Kato et al.,* 2012], which might be valuable for the risk assessment of intraplate faults. The search for repeating earthquakes on intraplate active faults, by deploying much more sensitive seismic networks than present, may be a worthy challenge. Some creeping is naturally expected even for faults with high overall coupling typical of intraplate faults if we recall the rate and state friction law. The friction law implies that any fault under nonzero shear load necessarily has a nonzero creep (= slip) velocity [e.g., *Dieterich*, 1979; *Nakatani*, 2001; *Rice et al.,* 2001], suggesting a viable possibility that many intraplate faults are actually creeping; they are just creeping very slowly.

7. Conclusions

1. Of the 851 AEs that occurred for 2 months on a geological fault (Zebra fault) at 1 km depth in a gold mine in South Africa, 45% were identified as repeating earthquakes on the basis of waveform similarity and their close locations. They are the smallest repeating earthquakes identified as such on a geological fault, with a magnitude range of $-5.1 \leq M_w \leq -3.6$.
2. These repeaters occurred steadily at the same location with similar magnitudes, similar to the repeaters at plate boundaries. The repeaters found in the present study are likely the repeat ruptures of asperities loaded by the long-term aseismic slip of the surrounding region (background creep), which is the generally accepted mechanism for plate-boundary repeaters.

3. The coseismic stress drops for the repeaters evaluated by a spectral ratio technique were 3.5–66 MPa (logarithmic average ~16 MPa), which falls in the range of values (0.1–100 MPa) observed for normal (i.e., nonrepeater) earthquakes.
4. Application of the NJ formula to the repeaters of the Zebra fault yields a background creep rate that is considered to be too large, contradicting the survival over several years of the signal cables grouted in the 60 mm boreholes penetrating this fault. That is, the actual creep rate of this fault was much less than that evaluated by the NJ formula. In contrast, the lower bound estimation of the background creep, which was made by summing up the coseismic slips of the repeaters assuming the seismically evaluated stress drop (16 MPa logarithmic average), was small enough to be consistent with the survival of the cables. The actual amount of the background creep should be between the above two estimates, probably close to the latter estimation, suggesting that these repeaters occurred at strongly coupled patches.
5. If such repeaters exist on tectonically loaded faults, observation of very small repeaters should make it possible to detect fault creep at very low rates, down to, say, orders of 0.01 mm/year, in realistic observation periods (e.g., several years). Search for such very small repeating earthquakes on active faults, by deploying much more sensitive seismic networks, may be a worthy challenge.
6. Although the number of studied cases is few, we surmise that repeaters at intraplate faults follow similar scaling to the repeaters we observed on the Zebra fault, while plate boundary faults tend to follow the NJ formula, which requires either high stress drop or low seismic coupling at repeater patches for small repeating earthquakes.

Appendix A: Dependency of Waveform Amplitudes on M_w Among Repeating AEs

In the estimation of stress drop in section 4, we used seismic moment M_o that was evaluated by fitting the theoretical ω-square spectra to the observed spectra of AE sensors and accelerometers in *Naoi et al.* [2014]. The frequency response of the AE sensors was calibrated in situ by comparing records from a pair of an accelerometer and an AE sensor that are closely situated. The accuracy of M_o and M_w estimates depends on the calibration accuracy. In this appendix, we check the reliability of the M_o and M_w estimates by using the repeating earthquakes presently studied.

Green's functions between an AE sensor and sources, including directivity of the sensor, are common among AEs belonging to the same repeater group. For events i and j belonging to the same repeater group, the following relation holds.

$$\frac{S_i(f)}{S_j(f)} = \frac{\Omega_i(f)}{\Omega_j(f)}.$$

where $S_i(f)$ and $S_j(f)$ are spectra of the observed records at an AE station for events i and j, respectively, and $\Omega_i(f)$ and$\Omega_j(f)$ are spectra of their source time functions. $\Omega(f)$ may be approximated by the ω-square model:

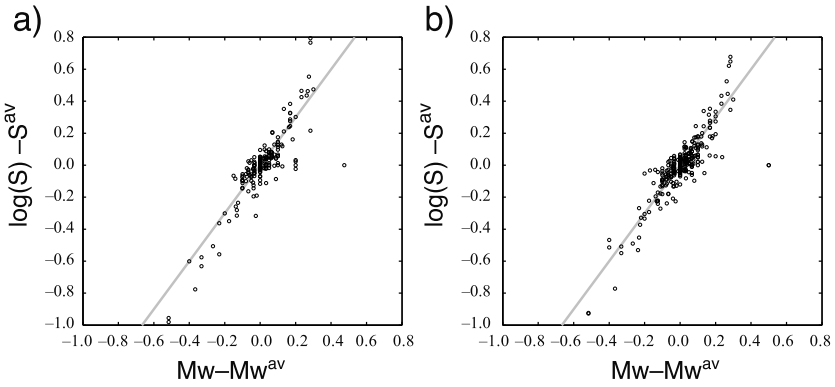

Figure A1. Comparison between the recorded amplitudes at an AE station and the moment magnitude M_w for all the repeaters identified in section 3 (except for events with low S/N ratio, see text). See Appendix A for the meaning of M_w^{av}, S, and S^{av}. (a) Result for *P* wave. (b) Result for *S* wave. Gray lines show the theoretical relation of slope 3/2.

$$\Omega(f) = \frac{M_O}{1 + \left(\frac{f}{f_c}\right)^2}.$$

Then, we obtain

$$\Omega(f_0) = M_O = 10^{\frac{3}{2}M_W + 9.1},$$

for a frequency f_o that is lower than f_c. From this relation, the logarithm of the spectral ratio $S_i(f_o)/S_j(f_o)$ is proportional to the difference of M_w:

$$\log \frac{S_i(f_0)}{S_j(f_0)} = \log S_i(f_0) - \log S_j(f_0) = \frac{3}{2}\left(M_W^i - M_W^j\right).$$

By summing up this equation with respect to j for all the events belonging to the same group, we obtain

$$\frac{1}{n}\sum_{j=1}^{n}\left(\log S_i(f_0) - \log S_j(f_0)\right) = \frac{1}{n}\sum_{j=1}^{n}\left(\frac{3}{2}\left(M_W^i - M_W^j\right)\right),$$

where n is the number of AEs in the repeater group. This can be rearranged into

$$\log S_i(f_0) - \frac{1}{n}\sum_{j=1}^{n}\left(\log S_j(f_0)\right) = \frac{3}{2}\left(M_W^i - \frac{1}{n}\sum_{j=1}^{n} M_W^j\right).$$

After rewriting the second term of the left-hand side to S^{av} (logarithmic average of $S(f_o)$ for all the events in the group) and the second term of the right-hand side to $M_w{}^{av}$ (average M_w), we obtain

$$\log S_i(f_0) - S^{av} = \frac{3}{2}\left(M_W^i - M_W^{av}\right).$$

We examined whether the presently studied repeaters satisfy this relation. Figure A1 represents the relation between $M_w{}^i$–$M_w{}^{av}$ and $\log S_i(f_o)$–S^{av} at an AE station for all the events identified to be repeaters in section 3. $S_i(f_0)$ were calculated by taking the peak-to-peak amplitude in a 2 ms window containing P or S wave (a window for P wave is shortened when it contains S wave), after applying a 2–5 kHz band-pass filter to the recorded waveforms. The records of low S/N ratio (<3) were precluded. The results for the P and S waves were both consistent with the theoretical relation of the slope of 3/2, indicating the reliable estimation of M_o and M_w.

Acknowledgments

We thank two reviewers for constructive comments. We thank Sibanye Gold Ltd., operator of the Cooke 4 mine, for approving our publication, and personnel at the mine and at the Institute of Mine Seismology for facilitating our project. We also thank Sylvester Morema, Sifiso Khambule, Joachim Philipp, Koji Miyakawa, Atsushi Watanabe, and late Gilbert Morema for their contribution to the observation. This project was funded by JSPS KAKENHI grants 21224012, 21246134, 26249137, and 26887022. It was also funded by JST/JICA, SATREPS and the MEXT's Earthquake and Volcano Hazards Observation and Research Program. R.J.D. acknowledges support from the South African Research Chairs Initiative of the Department of Science and Technology and the National Research Foundation. The waveform data and the event catalog used in the manuscript are not open to public because they were obtained in a working mine owned by a commercial company.

References

Aki, K. (1972), Earthquake mechanism, *Tectonophysics*, *13*, 423–446, doi:10.1016/0040-1951(72)90032-7.

Allmann, B. P., and P. M. Shearer (2007), Spatial and temporal stress drop variations in small earthquakes near Parkfield, California, *J. Geophys. Res.*, *112*, B04305, doi:10.1029/2006JB004395.

Beeler, N. M., D. L. Lockner, and S. H. Hickman (2001), A simple stick-slip and creep-slip model for repeating earthquakes and its implication for microearthquakes at Parkfield, *Bull. Seismol. Soc. Am.*, *91*, 1797–1804.

Chen, K. H., R. M. Nadeau, and R. J. Rau (2007), Towards a universal rule on the recurrence interval scaling of repeating earthquakes?, *Geophys. Res. Lett.*, *34*, L16308, doi:10.1029/2007GL030554.

Chen, K. H., R. M. Nadeau, and R. J. Rau (2008), Characteristic repeating earthquakes in an arc-continent collision boundary zone: The Chihshang fault of eastern Taiwan, *Earth Planet. Sci. Lett.*, *276*, 262–272, doi:10.1016/j.epsl.2008.09.021.

Chen, T., and N. Lapusta (2009), Scaling of small repeating earthquakes explained by interaction of seismic and aseismic slip in a rate and state fault model, *J. Geophys. Res.*, *114*, B01311, doi:10.1029/2008JB005749.

Dieterich, J. H. (1979), Modeling of rock friction: 1. Experimental results and constitutive equations, *J. Geophys. Res.*, *84*, 2161–2168, doi:10.1029/JB084iB05p02161.

Dreger, D., R. M. Nadeau, and A. Chung (2007), Repeating earthquake finite source models: Strong asperities revealed on the San Andreas fault, *Geophys. Res. Lett.*, *34*, L23302, doi:10.1029/2007GL031353.

Eshelby, J. D. (1957), The determination of the elastic field of an ellipsoidal inclusion, and related problems, *Proc. R. Soc. London, Ser. A*, *241*, 376–396.

Hayashi, M., and Y. Hiramatsu (2013), Spatial distribution of similar aftershocks of a large inland earthquake, the 2000 Western Tottori earthquake, in Japan, *Earth Planets Space*, *65*, 1587–1592, doi:10.5047/eps.2013.09.002.

Hiramatsu, Y., M. Hayashi, A. Hayashi, and the Group for the Joint Aftershock Observations of the 2007 Noto Hanto Earthquake (2011), Relation between similar aftershocks and ruptured asperity of a large inland earthquake: Example of the 2007 Noto Hanto earthquake, *Earth Planets Space*, *63*, 145–149, doi:10.5047/eps.2010.11.010.

Horiuchi, S., Y. Horiuchi, Y. Iio, Y. Sawada, S. Sekine, H. Nakamura, T. Okada, M. Nakatani, and M. Naoi (2011), Automatic *P* and *S* wave arrival time picking compared to manually picking, paper 3430 presented at IUGG General Assembly, Melbourne, Australia.

Hough, S. E. (1997), Empirical Green's function analysis: Taking the next step, *J. Geophys. Res.*, *102*, 5369–5384, doi:10.1029/96JB03488.

Ide, S., and G. C. Beroza (2001), Does apparent stress vary with earthquake size?, *Geophys. Res. Lett.*, *28*, 3349–3352, doi:10.1029/2001GL013106.

Ide, S., G. C. Beroza, S. G. Prejean, and W. L. Ellsworth (2003), Apparent break in earthquake scaling due to path and site effects on deep borehole recordings, *J. Geophys. Res., 108*(B5), 2271, doi:10.1029/2001JB001617.
Igarashi, T. (2010), Spatial changes of interplate coupling inferred from sequences of small repeating earthquakes in Japan, *Geophys. Res. Lett.*, *37*, L20304, doi:10.1029/2010GL044609.
Igarashi, T., T. Matsuzawa, and A. Hasegawa (2003), Repeating earthquakes and interplate aseismic slip in the northeastern Japan subduction zone, *J. Geophys. Res., 108*(B5), 2249, doi:10.1029/2002JB001920.
Ishii, H., T. Yamauchi, and F. Kusumoto (1997), Development of high sensitivity bore hole strain meters and application for rock mechanics and earthquake prediction study, in *Proceeding of 2nd International Symposium on Rock Stress*, edited by K. Sugawara and Y. Obara, pp. 253–258, A. A. Balkema, Rotterdam, Netherlands.
Johnson, L. R., and R. M. Nadeau (2002), Asperity model of an earthquake: Static problem, *Bull. Seismol. Soc. Am.*, *92*, 672–686, doi:10.1785/0120000282.
Kanamori, H., and D. L. Anderson (1975), Theoretical basis of some empirical relations in seismology, *Bull. Seismol. Soc. Am.*, *65*, 1073–1095.
Kato, A., K. Obara, T. Igarashi, H. Tsuruoka, S. Nakagawa, and N. Hirata (2012), Propagation of slow slip leading up to the 2011 M_w 9.0 Tohoku-Oki earthquake, *Science*, *335*, 705–708, doi:10.1126/science.1215141.
Keilis-Borok, V. I. (1959), On the estimation of the displacement in an earthquake source and of source dimensions, *Ann. Geophys.*, *12*, 205–214.
Kwiatek, G., K. Plenkers, G. Dresen, and JAGUARS Research Group (2011), Source parameters of picoseismicity recorded at Mponeng deep gold mine, South Africa: Implications for scaling relations, *Bull. Seismol. Soc. Am.*, *101*, 2592–2608, doi:10.1785/0120110094.
Matsuzawa, T., T. Igarashi, and A. Hasegawa (2002), Characteristic small-earthquake sequence off Sanriku, northeastern Honshu, Japan, *Geophys. Res. Lett., 29*(11), 1543, doi:10.1029/2001GL014632.
McGarr, A. (1999), On relating apparent stress to the stress causing earthquake fault slip, *J. Geophys. Res.*, *104*, 3003–3011, doi:10.1029/1998JB900083.
Nadeau, R. M., and L. R. Johnson (1998), Seismological studies at Parkfield VI: Moment release rates and estimates of source parameters for small repeating earthquakes, *Bull. Seismol. Soc. Am.*, *88*, 790–814.
Nakatani, M. (2001), Conceptual and physical clarification of rate and state friction: Frictional sliding as a thermally activated rheology, *J. Geophys. Res.*, *106*, 13,347–13,380, doi:10.1029/2000JB900453.
Naoi, M., et al. (2014), Frequency-magnitude distribution of $-3.7 \leq M_w \leq 1$ mining-induced earthquakes around a mining front and *b*-value invariance with post-blast time, *Pure Appl. Geophys.*, *171*, 2665–2684, doi:10.1007/s00024-013-0721-7.
Naoi, M., et al. (2015a), Quasi-static slip patch growth to 20 m on a geological fault inferred from acoustic emissions in a South African gold mine, *J. Geophys. Res. Solid Earth*, *120*, 1692–1707, doi:10.1002/2014JB011165.
Naoi, M., et al. (2015b), Steady activity of microfractures on geological faults loaded by mining stress, *Tectonophysics*, *649*, 100–114, doi:10.1016/j.tecto.2015.02.025.
Ogasawara, H. (2013), Observational studies to mitigate seismic risks in mines, paper presented at 23th International Seminar, Inst. of Mine Seismol. Hobart, Australia, 19 March.
Ogasawara, H., H. Kato, G. Hofmann, D. Roberts, P. Piper, T. Clements, A. K. Ward, Y. Yabe, H. Yilmaz, and R. J. Durrheim (2014), BX CCBO in-situ stress measurements at earthquake prone areas in South African gold mines—A summary of mini-workshop on 13 Feb 2014, paper 14-7438 presented at 48th US Rock Mechanics/Geomechanics Symposium, Minneapolis.
Rice, J. R., N. Lapusta, and K. Ranjith (2001), Rate and state dependent friction and the stability of sliding between elastically deformable solids, *J. Mech. Phys. Solids*, *49*, 1865–1898, doi:10.1016/S0022-5096(01)00042-4.
Sato, T., and T. Hirasawa (1973), Body wave spectra from propagating shear cracks, *J. Phys. Earth*, *21*, 415–431.
Uchida, N., and T. Matsuzawa (2011), Coupling coefficient, hierarchical structure, and earthquake cycle for the source area of the 2011 off the Pacific coast of Tohoku earthquake inferred from small repeating earthquake data, *Earth Planets Space*, *63*, 675–679.
Uchida, N., T. Matsuzawa, T. Igarashi, and A. Hasegawa (2003), Interplate quasi-static slip off Sanriku, NE Japan, estimated from repeating earthquakes, *Geophys. Res. Lett., 30*(15), 1801, doi:10.1029/2003GL017452.
Uchida, N., A. Hasegawa, T. Matsuzawa, and T. Igarashi (2004), Pre- and post-seismic slip on the plate boundary off Sanriku, NE Japan associated with three interplate earthquakes as estimated from small repeating earthquake data, *Tectonophysics*, *385*, 1–15.
Uchida, N., J. Nakajima, A. Hasegawa, and T. Matsuzawa (2009), What controls interplate coupling? Evidence for abrupt change in coupling across a border between two overlying plate in the NE Japan subduction zone, *Earth Planet. Sci. Lett.*, *283*, 111–121, doi:10.1016/j.epsl.2009.04.003.
Uchida, N., T. Matsuzawa, W. L. Ellsworth, K. Imanishi, K. Shimamura, and A. Hasegawa (2012), Source parameters of microearthquakes on an interplate asperity off Kamaishi, NE Japan over two earthquake cycles, *Geophys. J. Int.*, *189*, 999–1014, doi:10.1111/j.1365-246X.2012.05377.x.
Waldhauser, F., and W. L. Ellsworth (2000), A double-difference earthquake location algorithm: Method and application to the northern Hayward fault, California, *Bull. Seismol. Soc. Am.*, *90*, 1353–1368, doi:10.1785/0120000006.
Yamada, T., J. Mori, S. Ide, H. Kawakata, Y. Iio, and H. Ogasawara (2005), Radiation efficiency and apparent stress of small earthquakes in a South African gold mine, *J. Geophys. Res.*, *110*, B01305, doi:10.1029/2004JB003221.
Yamada, T., J. J. Mori, S. Ide, R. E. Abercrombie, H. Kawakata, M. Nakatani, Y. Iio, and H. Ogasawara (2007), Stress drops and radiated seismic energies of microearthquakes in a South African gold mine, *J. Geophys. Res.*, *112*, B03305, doi:10.1029/2006JB004553.
Yamamoto, A. (2008), A 2-year repeating earthquake activity within 250 m from M_w 2–3 source area in the Bambanani gold mine, South Africa (in Japanese), MS thesis, Ritsumeikan Univ., Kusatsu, Japan.
Yoshimitsu, N., H. Kawakata, A. Yamamoto, H. Ogasawara, and Y. Iio (2012), Temporal changes in attenuation of *S* waves through a fault zone in a South African gold mine, *Geophys. J. Int.*, *191*, 1317–1324, doi:10.1111/j.1365-246X.2012.05678.x.
Yoshimitsu, N., H. Kawakata, and N. Takahashi (2014), Magnitude −7 level earthquakes: A new lower limit of self-similarity in seismic scaling relationships, *Geophys. Res. Lett.*, *41*, 4495–4502, doi:10.1002/2014GL060306.
Yu, W. (2013), Shallow-focus repeating earthquakes in the Tonga–Kermadec–Vanuatu subduction zones, *Bull. Seismol. Soc. Am.*, *101*, 463–486, doi:10.1785/0120120123.